DOI:
10.1148/radiol.13130502

Document Version
Publisher's PDF, also known as Version of record

Radiology

Vascular Remodeling and Plaque Vulnerability in a Rabbit Model of Atherosclerosis: Comparison of Delayed-Enhancement MR Imaging with an Elastin-specific Contrast Agent and Unenhanced Black-Blood MR Imaging[1]

Alkystis Phinikaridou, PhD
Marcelo E. Andia, MD, PhD[2]
Andreas Indermuehle, MD
David C. Onthank, PhD
Rick R. Cesati, PhD
Alberto Smith, PhD
Simon P. Robinson, PhD
Prakash Saha, PhD, MRCS
René M. Botnar, PhD

Purpose: To compare delayed-enhancement (DE) magnetic resonance (MR) imaging with an elastin-specific contrast agent and unenhanced black-blood (BB) MR imaging with regard to vessel wall delineation and assessment of vascular remodeling and to test the prospective value for predicting plaque disruption in a rabbit model of atherosclerosis.

Materials and Methods: All procedures were approved by the animal ethics committee. Atherosclerosis was induced in 14 New Zealand White rabbits by means of a 1% cholesterol diet and endothelial denudation. Plaque disruption was triggered with Russell's viper venom and histamine. Animals with atherosclerosis were imaged before triggering to identify plaques and vascular remodeling and after triggering to identify thrombus. Plaques were classified as nondisrupted (stable) or disrupted (vulnerable). Control rabbits fed a regular diet were imaged twice. Unenhanced T1-weighted BB MR imaging, DE MR imaging with an elastin-specific contrast agent, and T1 mapping were used to assess vascular remodeling and calculate the plaque area and vessel wall relaxation rate (R1 = 1/T1). Elastin was quantified by using elastica–van Gieson stain. Group comparisons were analyzed with the Mann-Whitney or paired *t* test. Agreement between methods was performed with Bland-Altman analysis.

Results: Unenhanced T1-weighted BB MR imaging and DE MR imaging showed that, compared with nondisrupted plaques, disrupted plaques had larger plaque area (T1-weighted BB MR imaging: 5.1 mm^2 vs 5.7 mm^2; DE MR imaging: 6.0 mm^2 vs 7.9 mm^2; $P < .001$) and vessel area (T1-weighted BB MR imaging: 11.8 mm^2 vs 14.3 mm^2; DE MR imaging: 10.8 mm^2 vs 13.9 mm^2; $P < .001$) and underwent positive remodeling. Assessment of positive remodeling with DE MR imaging enabled better prediction of plaque disruption compared to that with unenhanced T1-weighted BB imaging (sensitivity: 83.7% vs 58.1%). DE MR imaging showed a stronger agreement with histologic findings, whereas the vessel area was overestimated with unenhanced T1-weighted BB imaging.

Conclusion: Compared with unenhanced T1-weighted BB MR imaging, DE MR imaging with an elastin-specific contrast agent enables more accurate assessment of vascular remodeling in the prediction of vulnerable plaque.

Online supplemental material is available for this article.

[1] From the Division of Imaging Science and Biomedical Engineering (A.P., M.E.A., A.I., R.M.B.), Academic Department of Surgery, Cardiovascular Division (A.S., P.S.), BHF Centre of Excellence, Cardiovascular Division (A.P., A.S., P.S., R.M.B.), and Wellcome Trust and EPSRC Medical Engineering Center (R.M.B.), King's College London, The Rayne Institute, 4th Floor, Lambeth Wing, St Thomas' Hospital, London SE1 7EH, England; and Lantheus Medical Imaging, North Billerica, Mass (D.C.O., R.R.C., S.P.R.). Received February 26, 2013; revision requested April 23; revision received June 24; accepted July 10; final version accepted October 8. Supported by the King's BHF Centre of Research Excellence (BHF RE/08/003) and National Institute for Health Research (NIHR) Biomedical Research Centre at Guy's and St Thomas' NHS Foundation Trust and King's College London. M.E.A. supported by the Redes-12-0026 grant from the Chilean Agency for Research in Science and Technology (CONICYT). P.S. supported by a Clinical Research Training Fellowship from the Wellcome Trust. R.M.B. supported by the British Heart Foundation (grant PG/10/044/28343). **Address correspondence to** A.P. (e-mail: *alkystis.1.phinikaridou@kcl.ac.uk*).

The views expressed are those of the authors and not necessarily those of the NHS, NIHR, or Department of Health.

[2] **Current address:** Department of Radiology, School of Medicine, Pontificia Universidad Católica de Chile, Santiago, Chile.

Atherosclerosis is the major cause of cardiovascular morbidity and mortality. Clinical events such as myocardial infarction are caused by rupture and/or erosion of "high-risk or vulnerable" lesions. Culprit lesions are characterized by a thin fibrous cap, large plaque burden, small luminal area, neovascularization, intraplaque hemorrhage, and expansive and/or positive vascular remodeling (1–5).

Magnetic resonance (MR) imaging is a noninvasive modality that enables imaging of the vessel wall with high spatial resolution. MR imaging without (6,7) and with (8–17) nonspecific contrast agents has been used for in vivo plaque characterization, quantification of plaque burden, endothelial permeability space, neovascularization, and assessment of vascular remodeling. Furthermore, MR imaging with targeted contrast agents has enabled direct visualization of biologic processes (18–23). However, the MR imaging techniques used are dependent on blood flow, the imaging protocols are lengthy, and imaging is limited to only certain segments of the coronary arteries. Consequently, vascular remodeling of the coronary arteries has been mainly assessed with use of invasive intravascular ultrasonography (US) and/or multidetector computed tomography (3–5,24). A flow-independent delayed-enhancement (DE) MR imaging protocol that was clinically established for myocardial infarction imaging and has been used for coronary vessel wall imaging in humans (9,10,25) could be beneficial for the assessment of vascular remodeling compared with blood flow–dependent black-blood (BB) MR imaging protocols.

We hypothesize that the abundance of elastin in the vessel wall (23,26) would enable more accurate segmentation of the wall contours, particularly the adventitial vessel wall contour, which is crucial for the classification of vascular remodeling. We performed this study to compare DE MR imaging with an elastin-specific contrast agent and unenhanced BB MR imaging with regard to vessel wall delineation and assessment of vascular remodeling and to test the prospective value for predicting plaque disruption in a rabbit model of atherosclerosis (23,25,27).

Advances in Knowledge

- Delayed-enhancement (DE) MR imaging with a flow-independent sequence after the administration of an elastin-specific contrast agent enabled more accurate assessment of vascular remodeling for the detection of "high-risk or vulnerable" atherosclerotic plaque compared with a standard unenhanced T1-weighted black-blood (BB) sequence in the rabbit model of accelerated atherosclerosis and experimentally induced plaque disruption (sensitivity: 83.7% vs 58.1%).
- Bland-Altman comparison of in vivo MR imaging and corresponding ex vivo histologic measurements showed that DE MR imaging with an elastin-specific contrast agent enabled more accurate segmentation of the outer and/or adventitial vessel wall contour compared with unenhanced T1-weighted BB MR imaging and, therefore, better assessment of vascular remodeling.
- DE MR imaging with an elastin-specific contrast agent showed significantly greater uptake in atherosclerotic plaque compared with normal rabbit vessel walls (R1: 2.37 sec^{-1} vs 1.62 sec^{-1}; P = .02), which was in good agreement with the histologic accumulation of elastin fibers in the neointima (36.1% of total area vs 26.0% of total area; P = .02).

Implications for Patient Care

- The use of a DE flow-independent protocol that is clinically accepted for myocardial infarction imaging and has been used for coronary plaque imaging makes the findings of this preclinical study highly translatable to vessel wall imaging in humans should the contrast agent be approved for human use.
- Such application may enable noninvasive assessment of plaque burden and vascular remodeling of human atherosclerosis; importantly, it may enable the study of the association of these measurements with plaque progression and instability in a serial and/or longitudinal manner.

Materials and Methods

The elastin-specific contrast agent was provided by Lantheus Medical Imaging (North Billerica, Mass). D.C.O., R.R.C., and S.P.R. are employees of Lantheus. Those authors who are not employees of or consultants for that industry (A.P., M.E.A., P.S., A.S., A.I., R.M.B.) had control of inclusion of data and information that might present a conflict of interest for the industry authors.

Animal Experiment Protocol

All procedures were approved by the animal ethics committee and performed according to the United Kingdom Animals (Scientific Procedures) Act 1986. Fourteen 3-month-old male New Zealand White rabbits (Harlan, Wyton, England; mean weight, 2.5 kg) were fed a 1% cholesterol diet (Special Diet Services,

Published online before print
10.1148/radiol.13130502 **Content code:** CA

Radiology 2014; 271:390–399

Abbreviations:
BB = black blood
DE = delayed enhancement

Author contributions:
Guarantors of integrity of entire study, A.P., P.S., R.M.B.; study concepts/study design or data acquisition or data analysis/interpretation, all authors; manuscript drafting or manuscript revision for important intellectual content, all authors; manuscript final version approval, all authors; literature research, A.P., M.E.A.; clinical studies, A.I.; experimental studies, A.P., M.E.A., A.I., R.R.C., A.S., P.S.; statistical analysis, A.P., M.E.A.; and manuscript editing, A.P., M.E.A., A.I., R.R.C., A.S., S.P.R., P.S., R.M.B.

Conflicts of interest are listed at the end of this article.

Witham, England) for 2 weeks before and 6 weeks after balloon injury of the abdominal aorta. This was followed by 4 weeks of normal chow diet (Fig E1 [online]) (11,19,28–31). Diseased rabbits received intraperitoneal administration of Russell's viper venom (0.15 mg/kg; Enzyme Research Laboratories, Swansea, United Kingdom), a procoagulant factor, followed 30 minutes later by intravenous administration of histamine dihydrochloride (0.02 mg/kg; Sigma-Aldrich, Dorset, England), a vasoconstrictor in rabbits, to induce plaque disruption and thrombosis. This procedure was repeated twice within 4 hours. Two nonballoon injured, age- and sex-matched rabbits were fed a normal diet for 12 weeks and were used as controls. At this time, animals were imaged before and after the administration of the elastin-specific contrast agent within the same day.

Elastin-specific MR Contrast Agent

LMI1174 (Lantheus Medical Imaging) is a low-molecular-weight (855.95 Da) MR contrast agent with moderate specificity for elastin (half maximal inhibitory concentration, 0.33 mmol/L) and similar blood half-life time to that of currently used extracellular gadolinium-based MR contrast agents (<2% injected dose per gram after 60 minutes and complete blood clearance time by 2 hours). It is composed of a gadolinium diethylenetriamine pentaacetic acid chelate linked to the D-amino acid D-phenylalanine. At 3.0 T, the unbound fraction has a relaxivity of 4.3 L $\cdot$mmol^{-1} $\cdot$ sec^{-1}, whereas the bound fraction has a relaxivity of 8.2 L $\cdot$ mmol$^{-1}\cdot$ sec^{-1} (23,25,27).

In Vivo MR Imaging

The abdominal aorta of control and diseased animals was imaged with a 3.0-T MR unit (Achieva; Philips Healthcare, Best, the Netherlands) and a 32-channel cardiac coil. Rabbits received general anesthesia and were imaged in the supine position before and after pharmacologic triggering. The pretrigger MR imaging session included acquisition of precontrast (unenhanced) scout phase-contrast MR angiograms, T1-weighted BB images, inversion-recovery images, and T1 maps. Subsequently, DE inversion-recovery images and T1 maps were obtained approximately 3 hours after intravenous administration of 0.2 mmol/kg of the elastin-specific contrast agent. Finally, the posttriggering MR imaging session, performed approximately 10 hours after the pretrigger session, included acquisition of only scout images, phase-contrast angiograms, and unenhanced T1-weighted BB images to visualize thrombus. Only the diseased rabbits underwent posttriggering MR imaging.

Phase-contrast angiograms were acquired for visualization of the aorta, renal branches, and iliac bifurcation with the following parameters: repetition time msec/echo time msec, 20/3; 15° flip angle; 300 × 150-mm field of view; 256 × 122 matrix; 1.2 × 0.6 × 1-mm resolution; 20 sections; velocity-encoding value, 150 cm/sec; and two signals acquired. The maximum intensity projection images were used to plan the subsequent images. Electrocardiographically triggered unenhanced two-dimensional T1-weighted BB images were acquired with the following parameters: repetition time, two heartbeats; echo time, 5.4 msec; profile order of low-high; echo train length, six; BB delay of 350 msec; 120 × 85-mm field of view; 384 × 270 matrix; 0.31 × 0.31-mm resolution; 4-mm-thick sections; 25 sections; and two signals acquired. A two-dimensional Look-Locker sequence was used to determine the optimal inversion time for blood signal nulling before and after administration of the elastin-specific contrast agent with the following parameters: 8.5/3.8, 150 × 150-mm field of view, 152 × 150 matrix, 1 × 1 × 10-mm resolution, and one section. Non–electrocardiographically gated inversion-recovery three-dimensional gradient-echo axial images were then acquired before and after administration of the elastin-specific contrast agent with the following parameters: 20/5.4; 120 × 85-mm field of view; 520 × 369 matrix; 0.23 × 0.23-mm resolution; 4-mm-thick sections; 25 sections; two signals acquired; repetition time between subsequent inversion-recovery pulses, 1000 msec; and 30° flip angle. T1 mapping was performed before and after administration of the elastin-specific contrast agent by using a gradient-echo sequence that employs two nonselective inversion pulses with inversion times ranging from 20 to 2000 msec, followed by eight segmented readouts for eight individual images. T1 mapping parameters were as follows: 3.5/1.8, 10° flip angle, 0 × 58-mm field of view, 116 × 70 matrix, 0.7 × 0.8-mm resolution, 3-mm-thick sections, 15 sections, and one signal acquired (23,32).

After the final MR imaging session, rabbits were euthanized with intravenous injection of a bolus of sodium pentobarbital (100 mg/kg) and aortas were extracted. During extraction, the aortas were marked with suture ligature at distances above and below the left renal branch that matched the total length covered by the in vivo MR imaging sections. Before the vessels were cut, the total length was measured with a ruler, and the vessel was marked with ink on its anterior site at every 2 cm. After extraction, the ligatures were used to re-extend the aortas to their physiologic length, and the ink marks were used to stretch the vessel equally such that the ink marks were retained at 2-cm intervals. Subsequently, the tissue was fixed with 10% formalin solution (Thermo Scientific, Waltham, Mass).

MR Image Analysis

Unenhanced T1-weighted BB MR images and DE MR images obtained before pharmacologic triggering were evaluated for plaque disruption; posttrigger images were used only to detect mural thrombus. Images from pretrigger unenhanced T1-weighted BB MR imaging and DE MR imaging were used to manually segment the vessel area (defined by the adventitial contour) and the lumen area by using image processing software (OsiriX; OsiriX Foundation, Geneva, Switzerland). Plaque area was calculated by subtracting lumen area from vessel area. Cross-sectional narrowing was calculated as follows: (plaque area/vessel area) × 100%.

Vascular remodeling was assessed on images from pretrigger unenhanced

T1-weighted BB MR imaging and DE MR imaging on the basis of the outer vessel wall area measured in the abdominal aorta. Two times the standard deviation from the linear regression line of the vessel area measured on consecutive sections covering the abdominal aorta was used as the cutoff point. Vascular remodeling was classified as positive, negative, or intermediate when the vessel area was larger than the upper 95% confidence band (vessel area more than +2 SD), smaller than the lower 95% confidence band (vessel area less than −2 SD), or within the 95% confidence band (vessel area was at least −2 SD and less than or equal to +2 SD), respectively. Pretrigger T1 maps were used to calculate the vessel wall relaxation rate (R1, in sec^{-1}) before and after administration of the elastin-specific contrast agent on a pixel-by-pixel basis by using in-house software (Matlab, Natick, Mass) (23). Posttrigger unenhanced T1-weighted BB images were only used to identify the presence or absence of thrombus as an end point for the classification of plaques as disrupted or nondisrupted, respectively (11,31). Analysis of MR images was performed by two independent readers (A.P. and M.E.A., both with more than 10 years of experience).

Histologic Analysis

En face preparations of the aorta were used to visualize atherosclerosis, vascular remodeling, and thrombus. Transverse cryosections (10 μm thick) were collected throughout the length of each segment at 500-μm intervals and stained with Masson trichrome for cellular components collagen, thrombus, and vascular measurements. Elastica–van Gieson stain was used to visualize the elastin fibers and calculate the elastin content (neointima and media area). Vessel and lumen areas, which are defined by the adventitial and luminal contours, were manually segmented with ImageJ software (National Institutes of Health, Bethesda, Md). The plaque area was calculated from the difference of these measurements. Computer-assisted color image analysis (ImageJ) was used to quantify the vascular elastin area, which was expressed in square millimeters or as a percentage of total elastin ([elastica van Gieson–stained area/adventitial area] × 100). Control aorta (six segments from the two control rabbits) and diseased aorta (20 plaque-bearing segments from the 14 diseased animals) were used for the analysis of the percentage elastin content of the tissue. For registration of the in vivo MR images and histologic sections, the distance of the proximal end of each segment from the renal branches and iliac bifurcation, the gross morphology, and internal plaque and/or thrombus landmarks visible on both the MR and histologic images were used as references. Histologic analysis was performed by A.P., who has more than 10 years of experience.

Statistical Analysis

Software (The Statistical Package for the Social Sciences 19.0; IBM, Somers, NY) was used for statistical analysis. For two-group comparisons, continuous variables were compared with a Mann-Whitney nonparametric test (MR imaging–derived measurements between stable vs vulnerable plaque, R1 after contrast material administration between control and diseased aortas, percentage total elastin in control vs diseased sections). R1 values before and after contrast material administration were compared by using a paired *t* test. Correlation analysis was performed by using the Spearman test. The agreement between in vivo MR imaging measurements and histologic findings was assessed by using Bland-Altman plots. The predictive value of unenhanced T1-weighted BB and DE MR imaging in the prediction of plaque disruption was assessed by using sensitivity, specificity, positive and negative predictive values, and the receiver operating characteristic curve. The McNemar exact test was used to compare the sensitivities, specificities, and accuracies of positive remodeling assessed with DE MR imaging and unenhanced T1-weighted BB imaging to correctly identify disrupted plaque. Logistic regression analysis was used to identify independent predictors of plaque disruption, with the presence or absence of thrombus as the outcome variable. Data are presented as medians and interquartile ranges. $P < .05$ was considered indicative of a significant difference.

Results

MR Imaging of Atherosclerosis and Plaque Classification

Atherosclerosis was observed in all 14 injured and cholesterol-fed rabbits, and thrombosis occurred in seven (50%). No atherosclerosis was observed in control rabbits. Posttriggered MR images from the 14 diseased animals demonstrated that 42 of 284 vessel wall segments or sections (14.8%) had thrombus and 242 (85.2%) did not. Representative unenhanced T1-weighted BB MR images and histologic images of the aorta from the same animal are shown in Figure 1. Vessel wall thickening (vessel wall area: 6.0 mm^2 for nondisrupted plaque and 7.0 mm^2 for disrupted plaque) is seen on the pretriggered images, whereas mural thrombus is seen only on the posttriggered image of the disrupted plaque. The vessel wall area was 2.4 mm^2 (range, 2.2–2.4 mm^2) in control animals and 6.7 mm^2 (range, 5.3–8.2 mm^2) in diseased animals.

MR Imaging with the Elastin-Binding Contrast Agent

Strong aortic wall enhancement was observed on DE MR images in both control and diseased animals (Fig 2). Vessel wall contours and thickness were more readily visualized on DE MR images (Fig 2, *B*, *F*, *C*, and *G*) than on precontrast images (Fig 2, *A* and *E*). Contrast enhancement of the vessel wall was quantified by using R1 relaxation maps (Fig 2, *D* and *H*). Quantitative measurements with pretrigger unenhanced T1-weighted BB images and DE MR images demonstrated a significantly larger vessel, lumen, and plaque area and a similar percentage of cross-sectional narrowing in disrupted compared with nondisrupted plaque from diseased animals (Table 1).

Figure 1

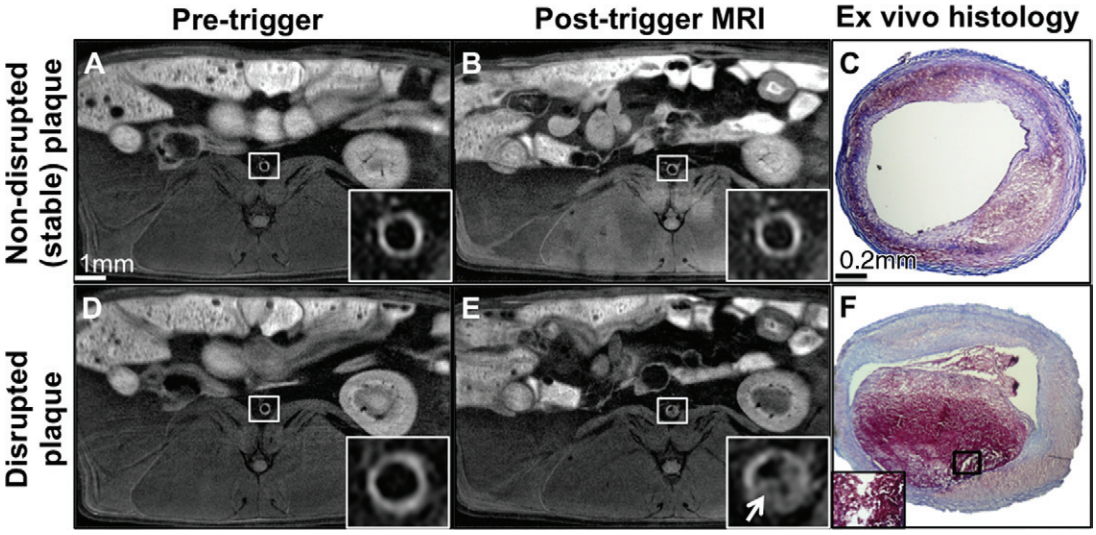

Figure 1: Images of atherosclerosis and disrupted and nondisrupted plaque. *A, D*, Cross-sectional unenhanced T1-weighted BB images obtained before pharmacologic triggering show vessel wall thickening. *B, E*, Corresponding images obtained after triggering for plaque disruption show presence of thrombus (arrow) overlying disrupted plaque. *C, F*, Photomicrographs (Masson trichrome stain; original magnification, ×2.5) show atherosclerosis and thrombus.

Figure 2

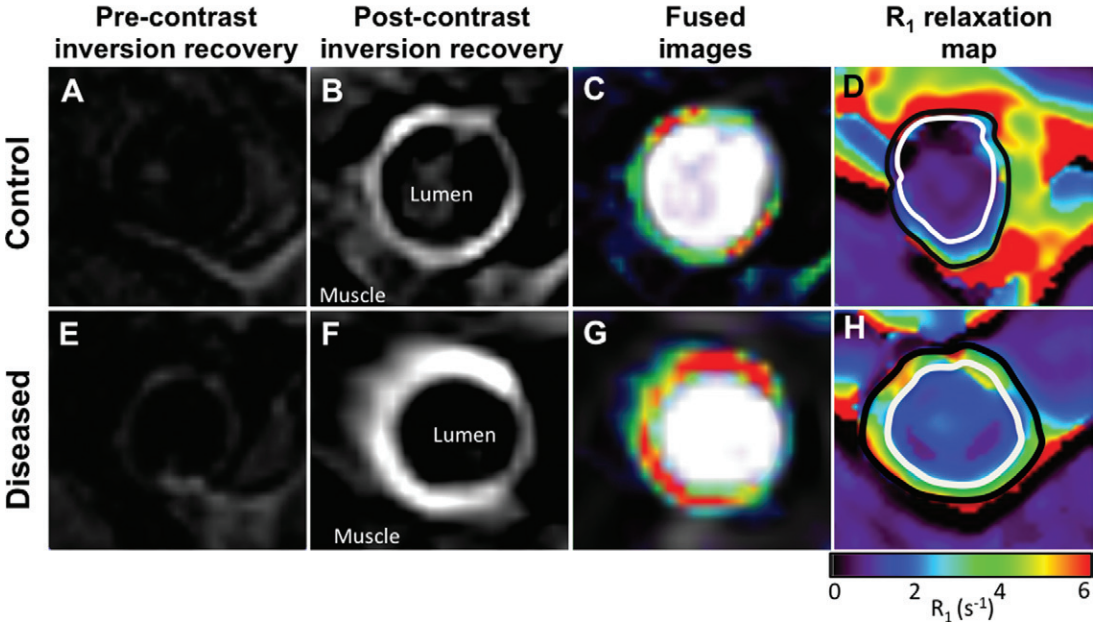

Figure 2: *A, E*, Cross-sectional precontrast MR images. *B, F*, Corresponding DE MR images obtained after administration of elastin-specific contrast agent. *C, G*, DE MR images fused with angiographic images. *D, H*, Corresponding R1 maps obtained after administration of elastin-specific contrast agent. Uptake of elastin-specific contrast agent and R1 values are higher in diseased compared with control aortas.

Table 1

Quantitative MR Imaging Measurements of Nondisrupted and Disrupted Plaques in Diseased Animals

Variable	Nondisrupted Plaque (n = 242)*	Disrupted Plaque (n = 42)*	P Value
Unenhanced T1-weighted BB imaging			
Vessel area (mm^2)	11.8 (9.4–13.9)	14.3 (11.0–20.6)	<.001
Lumen area (mm^2)	6.4 (5.0–8.2)	8.1 (5.7–9.8)	.002
Plaque area (mm^2)	5.1 (4.2–6.2)	5.7 (4.8–8.9)	.001
Cross-sectional narrowing (%)	44.3 (37.4–50.1)	46.6 (34.8–50.5)	.62
DE MR imaging			
Vessel area (mm^2)	10.8 (8.9–12.8)	13.9 (10.9–16.9)	<.001
Lumen area (mm^2)	4.4 (3.4–6.5)	6.4 (4.6–8.4)	<.001
Plaque area (mm^2)	6.0 (5.2–7.0)	7.9 (6.0–9.7)	<.001
Cross-sectional narrowing (%)	55.9 (47.4–63.1)	54.6 (45.2–59.9)	.22
Phase-contrast angiography			
Lumen area (mm^2)	5.3 (4.6–6.6)	5.6 (4.9–7.4)	.10

* Data are medians, with interquartile ranges in parentheses.

Histologic Examination

Elastin fibers (purple staining) were present in the media of control vessels (Fig 3, *A* and *D*) and in the neointima of atherosclerotic vessels (Fig 3, *B*, *C*, *E*, and *F*), as seen with elastica–van Gieson staining (percentage of total area: 26.0% [range, 25.0%–28.0%] vs 36.1% [range, 22.8%–47.8%], P = .02; Fig 3, *G*).

Vessel Wall Relaxation Rate and Enhancement Area at MR Imaging

Vessel wall R1 (Fig E2, *A* [online]) on images obtained after administration of the elastin-specific contrast agent was significantly higher than that on precontrast images ($P < .01$). Vessel wall R1 was also significantly higher in diseased compared with control vessels (median R1 for abdominal aorta: 2.37 sec^{-1} [range, 2.0–2.7 sec^{-1}] vs 1.62 sec^{-1} [range, 1.48–1.72 sec^{-1}], P = .02; median R1 for thoracic aorta: 1.95 sec^{-1} [range, 1.8–2.2 sec^{-1}] vs 1.6 sec^{-1} [range, 1.5–1.7 sec^{-1}], P = .03). The vessel wall R1 correlated strongly with the percentage total elastin content (r = 0.88; $P < .01$; 95% confidence interval: 0.62, 0.97; Fig E2, *B* [online]). Furthermore, the total elastin area showed a positive correlation with the enhanced area measured with DE MR imaging (r = 0.74; $P < .01$; 95% confidence interval: 0.29, 0.92; Fig E2, *C* [online]).

Disrupted Plaques Undergo Positive Vascular Remodeling

Representative pretrigger DE MR images obtained after administration of the elastin-specific contrast agent at four levels of the aorta (lines on the ex vivo specimen [Fig 4, *E*]) show focal enlargement of the vessel area (Fig 4, *A–D*). Positive remodeling observed on DE MR images was verified histologically (Fig 4, *E*), and the thrombus was confirmed when the vessel was opened longitudinally (Fig 4, *F*). A representative scatterplot from one animal shows the changes in the vessel area along the aorta, starting from the left renal branch (0 mm) until the iliac bifurcation (87 mm), and the classification of vascular remodeling (Fig 4, *G*). Two vessel wall segments (regions 1 and 2) showed enlarged vessel area (greater than mean +2 SD) and were classified as showing positive remodeling. Both regions contained plaques that disrupted after pharmacologic triggering. The rest of the data points correspond to regions of the aorta that contained nondisrupted plaques.

The predictive value of positive remodeling and plaque area, independently or in combination, in the detection of plaque disruption as measured on unenhanced T1-weighted BB images and DE MR images is shown in Table 2 and Tables E1 and E2 (online). The cutoff value for plaque area (≥5.7 mm^2) was calculated on the basis of the receiver operating characteristic curve as the value corresponding to the highest sensitivity and specificity in the prediction of plaque disruption. The presence of positive vascular remodeling at DE MR imaging had a higher sensitivity than the presence of positive vascular remodeling at unenhanced T1-weighted BB MR imaging in the detection of disrupted plaque (P = .04), whereas the specificity (P = .08) and accuracy (P = .9) were similar between the two imaging sequences. Logistic regression analysis identified plaque area and positive remodeling measured with DE MR imaging as predictors of plaque disruption (Tables E1, E2 [online]). There was good agreement between findings at in vivo MR imaging and ex vivo histologic examination, as shown with Bland-Altman analysis (Fig E3 [online]).

Discussion

Our study demonstrates that the use of a flow-independent inversion-recovery sequence for DE vessel wall imaging after administration of an elastin-specific MR contrast agent enabled more accurate assessment of vascular remodeling and detection of plaques with a higher likelihood to disrupt compared with the unenhanced T1-weighted BB images in a rabbit model of accelerated atherosclerosis and experimentally induced plaque disruption.

The specificity of the elastin-specific MR contrast agent was shown in ex vivo and in vivo settings (23,25,27). A gadolinium 153 (^{153}Gd)–labeled elastin agent showed preferential binding to purified elastin and little binding to bovine serum albumin and chondroitin-6-sulfate (25). Ex vivo and in vivo experiments showed that a ^{153}Gd-labeled elastin agent had high binding to normal and plaque-bearing arteries and co-localized with elastin fibers while showing little binding to rabbit vena cava with significantly lower elastin content (27).

Figure 3

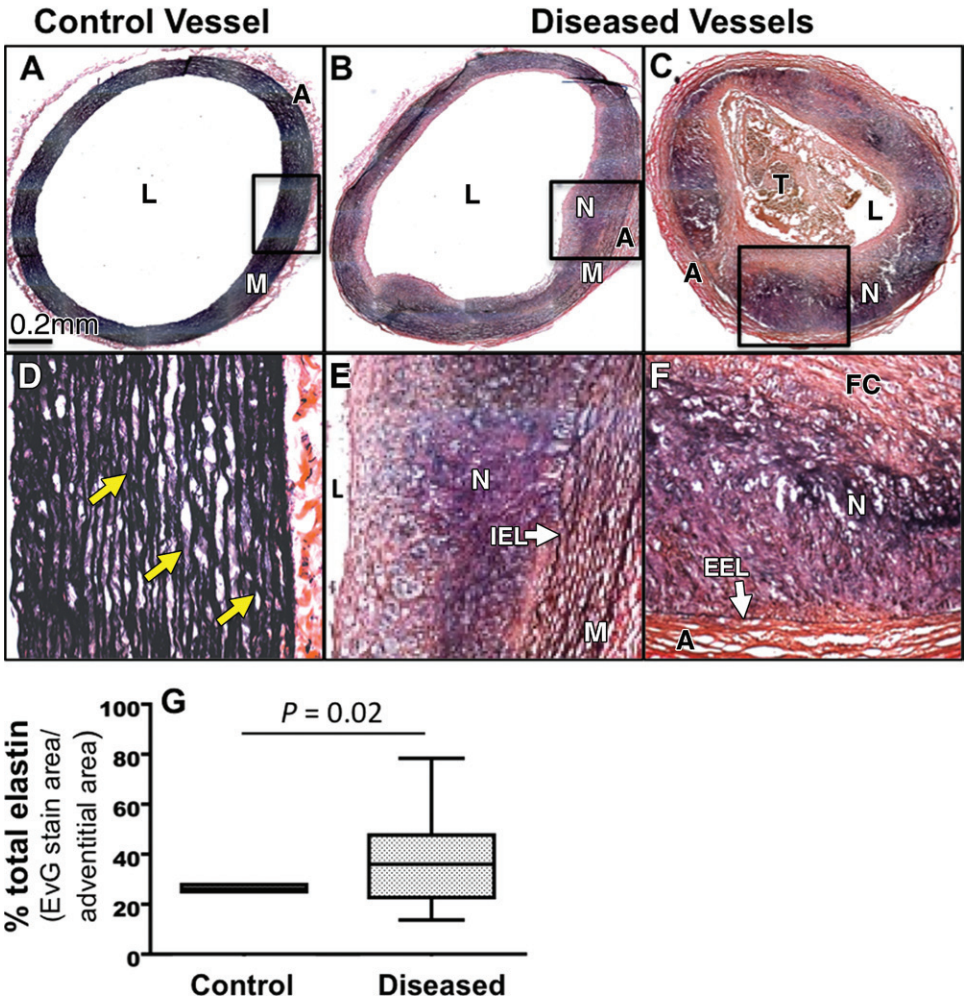

Figure 3: Histologic characteristics of elastin fibers. *D, E,* and *F* are magnifications (original magnification, ×10) of boxes in *A, B,* and *C* (original magnification, ×2.5). All photomicrographs were stained with Masson trichrome. *A, D,* Photomicrographs of control vessels show well-organized elastic fibers (purple-black) in media. Arrows in *D* indicate internal and external elastic lamina. *B, E, C, F,* Photomicrographs of diseased vessel walls show deposition of elastic fibers in neointima *(N)* overlying the internal elastic lamina *(IEL). G,* Quantification of percentage total elastin area. *A* = adventitia, *EEL* = external elastic lamina, *EvG* = elastica–van Gieson, *FC* = fibrous cap, *L* = lumen, *M* = media, *T* = thrombus.

An elastin-specific MR contrast agent was used for the first time to monitor image plaque burden in atherosclerotic apolipoprotein E–deficient mice (23) and later to image coronary artery remodeling after stent-induced injury in a swine model (25). In both studies, plaque burden measurements and the extent of vascular damage as assessed with DE MR imaging after administration of an elastin-specific contrast agent were in agreement with the vascular elastin content measured at histologic examination.

Herein, we further corroborated the finding that plaque progression is associated with the histologic accumulation of elastin fibers in the neointima that results in a significantly greater uptake of an elastin-specific MR contrast agent in atherosclerotic plaque compared with normal rabbit aorta. Importantly, the ability to experimentally induce plaque disruption and thrombosis at a precise time point provides a functional end point to classify plaque as nondisrupted and/or stable or disrupted and/or vulnerable. To this end, we were able to extent our study to compare the predictive value of the DE MR imaging after administration of an elastin-specific MR contrast agent with the commonly used unenhanced T1-weighted BB protocol in classifying vascular remodeling (negative, intermediate, and positive)

Figure 4

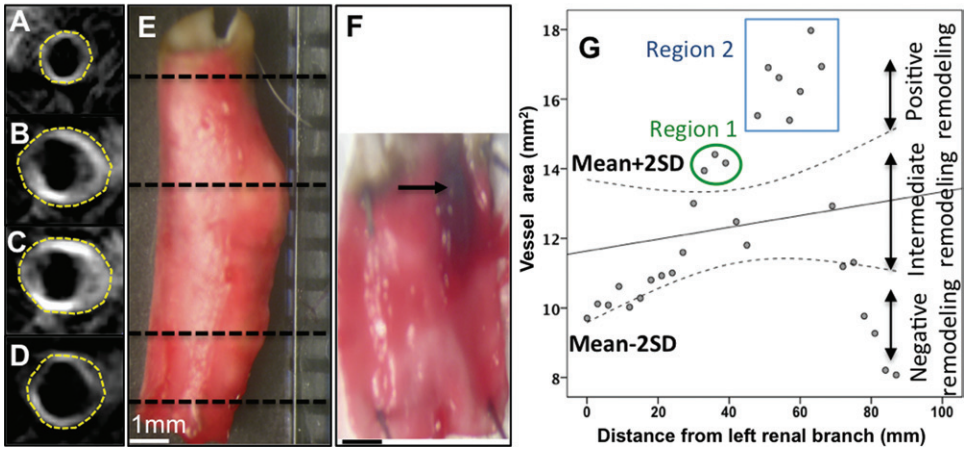

Figure 4: Positive vascular remodeling in disrupted plaques. *A–D*, DE MR images obtained after administration of elastin-specific contrast agent show positive remodeling, as defined by enlargement of vessel area (yellow contours). *E*, Corresponding en face photograph verifies presence of positive vascular remodeling. *F*, En face photograph of longitudinally open vessel shows thrombus (arrow) attached to vessel wall at proximal end of positive remodeling. *G*, Scatterplot shows change in vessel area measured on consecutive slices along aorta, starting from left renal branch (0 mm) to iliac bifurcation (86 mm). Two regions of the vessel wall underwent positive remodeling, with vessel areas falling above the mean + 2 SD margin. Both plaques disrupted after triggering. Four of seven sections covering the vulnerable region 2 are illustrated in *A–D*.

Table 2

Predictive Value of Positive Remodeling and Plaque Area in the Detection of Plaque Disruption

Variable	Sensitivity (%)	Specificity (%)	PPV (%)	NPV (%)	Diagnostic Accuracy (%)
Positive remodeling					
DE MR imaging	83.7 (69.3, 93.2)	91.8 (88.2, 94.6)	59.0 (45.7, 71.4)	97.6 (95.0, 99.0)	90.8 (87.6, 92.9)
Unenhanced T1-weighted BB imaging	58.1 (42.1, 73.0)	83.0 (77.7, 87.6)	37.9 (26.2, 50.7)	91.8 (87.3, 95.0)	79.3 (75.0, 83.2)
Plaque area at DE MR imaging*	88.4 (74.90, 96.07)	41.5 (35.17, 48.10)	21.6 (15.76, 28.41)	95.2 (89.03, 98.39)	48.7 (44.7, 51.0)
Both positive remodeling and plaque area at DE MR imaging*	72.0 (56.33, 84.66)	92.8 (88.72, 95.75)	64.6 (49.46, 77.83)	94.8 (91.10, 97.28)	89.6 (85.6, 92.8)

Note.–Data were obtained in 284 sections (242 nondisrupted and 42 disrupted plaques). Numbers in parentheses are 95% confidence intervals. Assessment of positive remodeling with DE MR imaging after administration of the elastin-specific contrast agent enabled a higher sensitivity, specificity, positive predictive value, negative predictive value, and diagnostic accuracy in the detection of plaque disruption compared to that with unenhanced T1-weighted BB imaging. The positive predictive value increased when both positive remodeling and plaque area (≥5.7 mm^2) were present. NPV = negative predictive value, PPV = positive predictive value.

* The cutoff value for plaque area was ≥5.7 mm^2.

for the detection of "high risk and/or vulnerable" plaque.

Both unenhanced T1-weighted BB images and DE MR images obtained with an elastin-specific MR contrast agent showed that a larger vessel, lumen, and plaque area are associated with disrupted plaque. However, assessment of vascular remodeling with the DE MR images showed higher predictive values for identifying disrupted plaques compared with the unenhanced T1-weighted BB technique. The strong uptake of the elastin-specific contrast agent in the aortic wall and the lack of uptake in the adjacent inferior vena cava and the paravertebral muscle owing to the inherently lower concentration or absence of elastin fibers, respectively, improved the segmentation of the adventitial vessel wall contour that is essential for accurate assessment of vascular remodeling (23,25,27). Assessment of remodeling with contrast material–enhanced MR imaging by using the standardized cutoff values established with intravascular US, instead of the 2 SD cutoff value as used herein, was previously reported by using the same rabbit model (11). In that study, vascular remodeling was assessed by using a bright-blood sequence after administration of a nonspecific gadolinium diethylenetriamine pentaacetic acid compound (Magnevist; Bayer Healthcare, Berlin, Germany) in which vessel

wall enhancement could be due to multiple factors (eg, increased distribution volume, inflammation, neovascularization), resulting in T1 shortening. The use of an elastin-specific contrast agent allowed the study of vascular remodeling by targeting the extracellular matrix and, compared with the previous method (11), provided higher sensitivity (83.7% vs 67.8%) and specificity (91.8% vs 77.6%) in the detection of plaques that disrupted after pharmacologic triggering.

One potential limitation of our study is whether experimentally induced plaque disruption in rabbits reflects spontaneous plaque rupture in humans. We (31) and others (28,29) have shown that plaque disruption after triggering occurs in plaques with well-established features of instability, including thin fibrous cap, large lipid core, inflammatory infiltrate, neovascularization, and positive remodeling (28,29,31). Precisely what triggers plaque disruption remains unclear. Studies have suggested that platelet activation and adhesion and the release of vasoconstriction molecules may be important (33,34). Therefore, the combination of a procoagulant factor (Russell's viper venom) and a vasoconstriction agent (histamine) may be an acceptable physiologic approximation.

Another limitation of our study might be that the in-plane resolution was higher with DE MR imaging (0.23 × 0.23 mm) than with unenhanced T1-weighted BB imaging (0.31 × 0.31 mm) and that partial volume effects might influence the accuracy of the measurements. However, the normal vessel wall in the rabbit aorta is approximately 0.5–0.6 mm thick; therefore, the in-plane resolution was sufficient to delineate the vessel wall with both the unenhanced T1-weighted BB and DE MR imaging sequences.

Practical application: Phase I and II clinical trials are currently being planned to investigate the merits of the elastin-binding contrast agent in humans with coronary atherosclerosis.

Disclosures of Conflicts of Interest: A.P. No relevant conflicts of interest to disclose. **M.E.A.** No relevant conflicts of interest to disclose. **A.I.** No relevant conflicts of interest to disclose. **D.C.O.** No relevant conflicts of interest to disclose. **R.R.C.** Financial activities related to the present article: none to disclose. Financial activities not related to the present article: none to disclose. Other relationships: has a patent with Lantheus Medical Imaging. **A.S.** No relevant conflicts of interest to disclose. **S.P.R.** Financial activities related to the present article: receives nonfinancial support from Lantheus Medical Imaging. Financial activities not related to the present article: is an employee of Lantheus Medical Imaging. Other relationships: has a patent with Lantheus Medical Imaging. **P.S.** No relevant conflicts of interest to disclose. **R.M.B.** No relevant conflicts of interest to disclose.

References

1. Virmani R, Kolodgie FD, Burke AP, Farb A, Schwartz SM. Lessons from sudden coronary death: a comprehensive morphological classification scheme for atherosclerotic lesions. Arterioscler Thromb Vasc Biol 2000;20(5):1262–1275.
2. Pasterkamp G, Schoneveld AH, van der Wal AC, et al. Relation of arterial geometry to luminal narrowing and histologic markers for plaque vulnerability: the remodeling paradox. J Am Coll Cardiol 1998;32(3):655–662.
3. Calvert PA, Obaid DR, O'Sullivan M, et al. Association between IVUS findings and adverse outcomes in patients with coronary artery disease: the VIVA (VH-IVUS in Vulnerable Atherosclerosis) Study. JACC Cardiovasc Imaging 2011;4(8):894–901.
4. Stone GW, Maehara A, Lansky AJ, et al. A prospective natural-history study of coronary atherosclerosis. N Engl J Med 2011;364(3):226–235.
5. Motoyama S, Sarai M, Harigaya H, et al. Computed tomographic angiography characteristics of atherosclerotic plaques subsequently resulting in acute coronary syndrome. J Am Coll Cardiol 2009;54(1):49–57.
6. Cai JM, Hatsukami TS, Ferguson MS, Small R, Polissar NL, Yuan C. Classification of human carotid atherosclerotic lesions with in vivo multicontrast magnetic resonance imaging. Circulation 2002;106(11):1368–1373.
7. Botnar RM, Stuber M, Kissinger KV, Kim WY, Spuentrup E, Manning WJ. Noninvasive coronary vessel wall and plaque imaging with magnetic resonance imaging. Circulation 2000;102(21):2582–2587.
8. Wasserman BA, Smith WI, Trout HH III, Cannon RO III, Balaban RS, Arai AE. Carotid artery atherosclerosis: in vivo morphologic characterization with gadolinium-enhanced double-oblique MR imaging—initial results. Radiology 2002;223(2):566–573.
9. Maintz D, Ozgun M, Hoffmeier A, et al. Selective coronary artery plaque visualization and differentiation by contrast-enhanced inversion prepared MRI. Eur Heart J 2006;27(14):1732–1736.
10. Yeon SB, Sabir A, Clouse M, et al. Delayed-enhancement cardiovascular magnetic resonance coronary artery wall imaging: comparison with multislice computed tomography and quantitative coronary angiography. J Am Coll Cardiol 2007;50(5):441–447.
11. Phinikaridou A, Ruberg FL, Hallock KJ, et al. In vivo detection of vulnerable atherosclerotic plaque by MRI in a rabbit model. Circ Cardiovasc Imaging 2010;3(3):323–332.
12. Pedersen SF, Thrysøe SA, Paaske WP, et al. CMR assessment of endothelial damage and angiogenesis in porcine coronary arteries using gadofosveset. J Cardiovasc Magn Reson 2011;13:10.
13. Phinikaridou A, Andia ME, Protti A, et al. Noninvasive magnetic resonance imaging evaluation of endothelial permeability in murine atherosclerosis using an albumin-binding contrast agent. Circulation 2012;126(6):707–719.
14. Yuan C, Kerwin WS, Ferguson MS, et al. Contrast-enhanced high resolution MRI for atherosclerotic carotid artery tissue characterization. J Magn Reson Imaging 2002;15(1):62–67.
15. Kim WY, Stuber M, Börnert P, Kissinger KV, Manning WJ, Botnar RM. Three-dimensional black-blood cardiac magnetic resonance coronary vessel wall imaging detects positive arterial remodeling in patients with nonsignificant coronary artery disease. Circulation 2002;106(3):296–299.
16. Miao C, Chen S, Macedo R, et al. Positive remodeling of the coronary arteries detected by magnetic resonance imaging in an asymptomatic population: MESA (Multi-Ethnic Study of Atherosclerosis). J Am Coll Cardiol 2009;53(18):1708–1715.
17. Astor BC, Sharrett AR, Coresh J, Chambless LE, Wasserman BA. Remodeling of carotid arteries detected with MR imaging: atherosclerosis risk in communities carotid MRI study. Radiology 2010;256(3):879–886.
18. Winter PM, Morawski AM, Caruthers SD, et al. Molecular imaging of angiogenesis in early-stage atherosclerosis with $\alpha_v\beta_3$-integ-

rin-targeted nanoparticles. Circulation 2003; 108(18):2270–2274.

19. Botnar RM, Perez AS, Witte S, et al. In vivo molecular imaging of acute and subacute thrombosis using a fibrin-binding magnetic resonance imaging contrast agent. Circulation 2004;109(16):2023–2029.
20. Amirbekian V, Lipinski MJ, Briley-Saebo KC, et al. Detecting and assessing macrophages in vivo to evaluate atherosclerosis noninvasively using molecular MRI. Proc Natl Acad Sci U S A 2007;104(3):961–966.
21. Ronald JA, Chen JW, Chen Y, et al. Enzyme-sensitive magnetic resonance imaging targeting myeloperoxidase identifies active inflammation in experimental rabbit atherosclerotic plaques. Circulation 2009;120(7):592–599.
22. Hyafil F, Vucic E, Cornily JC, et al. Monitoring of arterial wall remodelling in atherosclerotic rabbits with a magnetic resonance imaging contrast agent binding to matrix metalloproteinases. Eur Heart J 2011;32(12): 1561–1571.
23. Makowski MR, Wiethoff AJ, Blume U, et al. Assessment of atherosclerotic plaque burden with an elastin-specific magnetic resonance contrast agent. Nat Med 2011;17(3):383–388.
24. Schoenhagen P, Ziada KM, Kapadia SR, Crowe TD, Nissen SE, Tuzcu EM. Extent and direction of arterial remodeling in stable versus unstable coronary syndromes: an intravascular ultrasound study. Circulation 2000;101(6):598–603.
25. von Bary C, Makowski M, Preissel A, et al. MRI of coronary wall remodeling in a swine model of coronary injury using an elastin-binding contrast agent. Circ Cardiovasc Imaging 2011;4(2):147–155.
26. Krettek A, Sukhova GK, Libby P. Elastogenesis in human arterial disease: a role for macrophages in disordered elastin synthesis. Arterioscler Thromb Vasc Biol 2003;23(4):582–587.
27. Onthank D, Yalamanchili P, Cesati R, et al. BMS753951: a novel low molecular weight magnetic resonance contrast agent selective for arterial wall imaging [abstr]. Circulation 2007;116:II-411–II-412.
28. Constantinides P, Chakravarti RN. Rabbit arterial thrombosis production by systemic procedures. Arch Pathol 1961;72:197–208.
29. Abela GS, Picon PD, Friedl SE, et al. Triggering of plaque disruption and arterial thrombosis in an atherosclerotic rabbit model. Circulation 1995;91(3):776–784.
30. Johnstone MT, Botnar RM, Perez AS, et al. In vivo magnetic resonance imaging of experimental thrombosis in a rabbit model. Arterioscler Thromb Vasc Biol 2001;21(9): 1556–1560.
31. Phinikaridou A, Hallock KJ, Qiao Y, Hamilton JA. A robust rabbit model of human atherosclerosis and atherothrombosis. J Lipid Res 2009;50(5):787–797.
32. Blume U, Orbell J, Waltham M, Smith A, Razavi R, Schaeffter T. 3D T(1)-mapping for the characterization of deep vein thrombosis. MAGMA 2009;22(6): 375–383.
33. Golino P, Ashton JH, Buja LM, et al. Local platelet activation causes vasoconstriction of large epicardial canine coronary arteries in vivo: thromboxane A2 and serotonin are possible mediators. Circulation 1989;79(1):154–166.
34. Willerson JT, Golino P, Eidt J, Campbell WB, Buja LM. Specific platelet mediators and unstable coronary artery lesions: experimental evidence and potential clinical implications. Circulation 1989;80(1): 198–205.